

Size-Selective Collection of Circulating Tumor Cells using Vortex Technology

Elodie Sollier, Derek E. Go, James Che, Daniel R. Gossett, Sean O'Byrne, Westbrook M. Weaver, Nicolas Kummer, Matthew Rettig, Jonathan Goldman, Nicholas Nickols, Susan McCloskey, Rajan P. Kulkarni and Dino Di Carlo

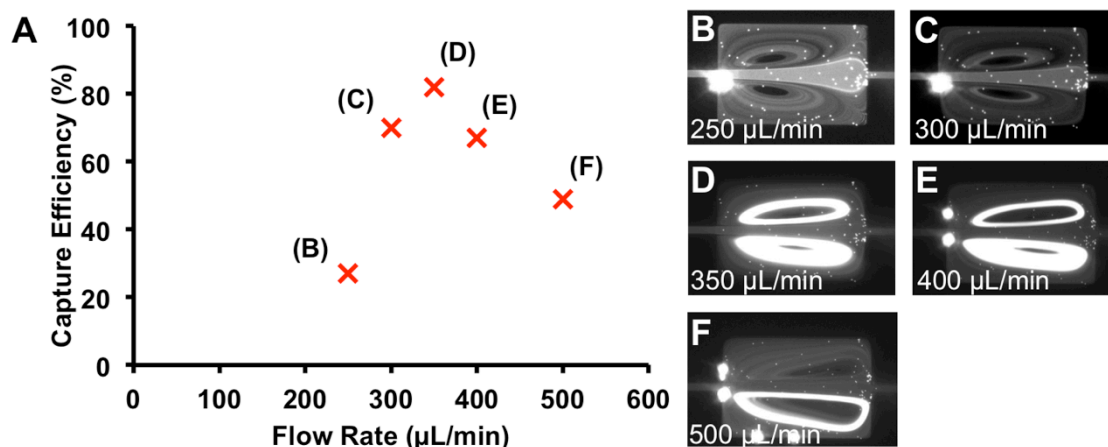


Figure S11. Effect of flow rate on vortex patterns and capture efficiency. As the flow rate increases from 250 to 350 $\mu\text{L}/\text{min}$, the vortices tend to occupy the reservoirs to a greater extent, and more beads are trapped in the larger orbits. Above 350 $\mu\text{L}/\text{min}$, the vortices occupy the whole extent available and the vortex center is progressively shifted towards the back wall of the reservoir: fewer particles enter in the vortices and the capture efficiency decreases.

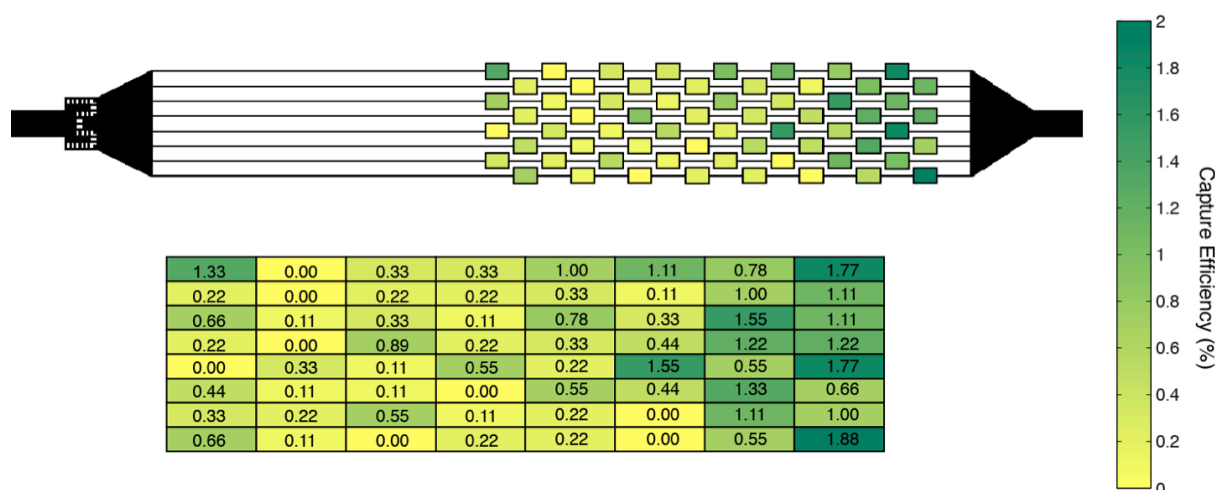


Figure S12. Capture efficiency along the microfluidic chip. When 19 μm rigid particles are injected through the device at 4 mL/min , the capture efficiency per reservoir is higher towards the end of the device. The table indicates the averaged capture efficiency in each reservoir, related to the total number of particles injected. ($N=3$, 300 particles injected, total capture efficiency of 35.3% for the device).

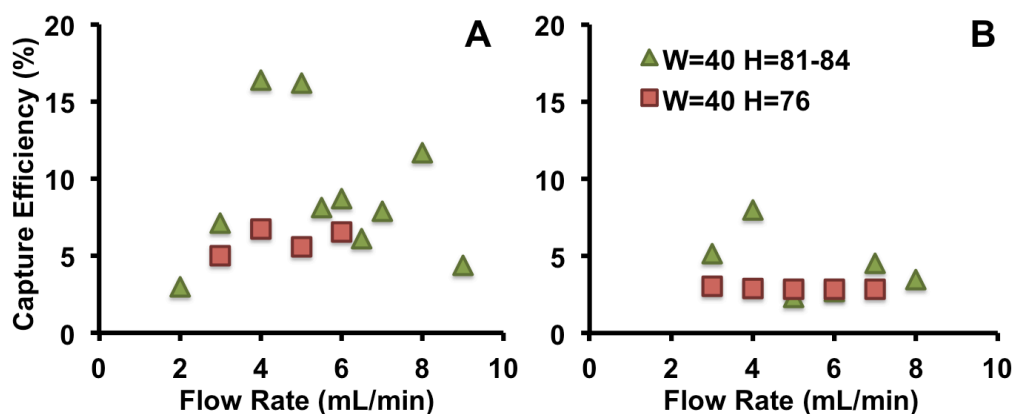


Figure S13. Experimental comparison of two devices for MCF7 breast cancer cells spiked in (A) PBS and (B) healthy blood. As illustrated in Figure 2, capture efficiency varies with channel aspect ratio and flow rate. As for rigid beads, taller channels (new device) provide an improvement in efficiency over devices used previously [1].

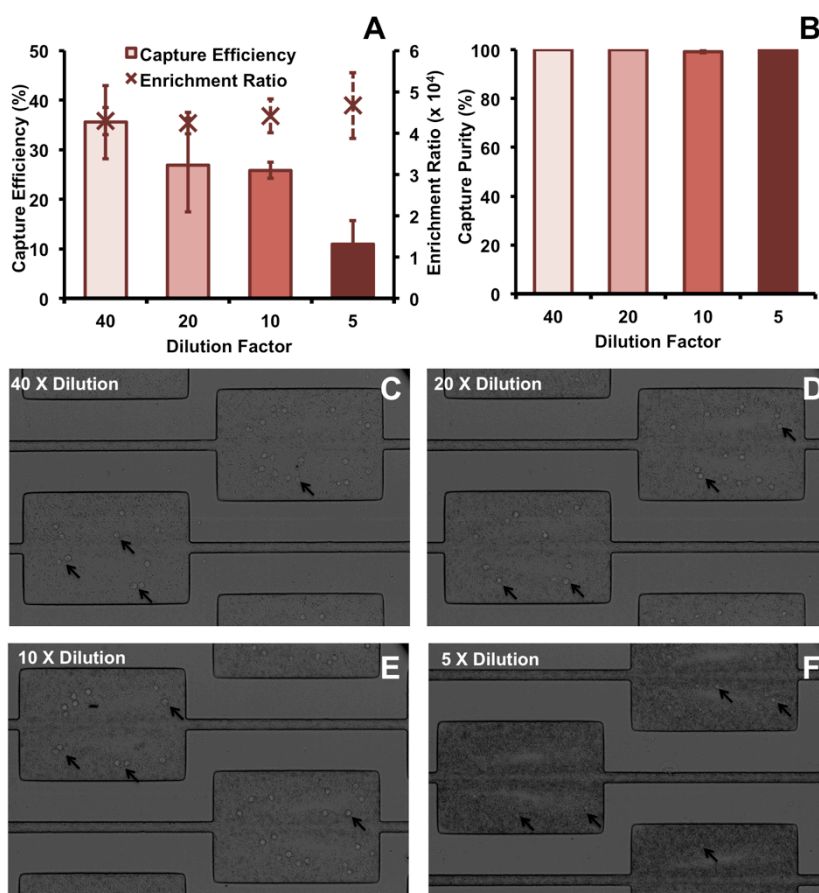


Figure S14. Effect of blood dilution on capture efficiency. Performance is assessed for MCF7 cells spiked in 5X, 10X, 20X and 40X diluted blood, with around 500 cells spiked in 0.5 mL of whole blood diluted with PBS. Three independent experiments are averaged. (A) Capture Efficiency and

Enrichment Ratio ($\times 10^4$) as a function of blood dilution. (B) Blood dilution has no effect on the capture purity. (C-F) High-speed pictures of cancer cell trapping from blood samples at different dilutions, 40X, 20X, 10X and 5X respectively.

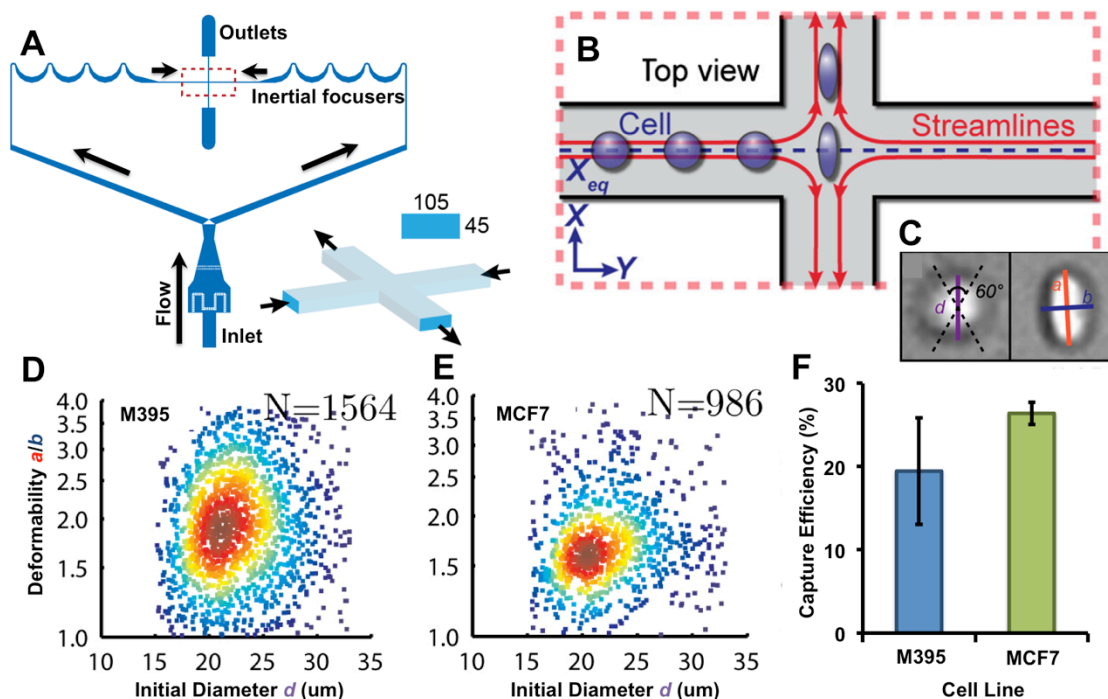


Figure SI5. Principles of Deformability Cytometry, modified from [2]. (A) Schematic of the microfluidic device (105 μm large by 45 μm high). Cells are focused to the channel centerline with the inertial focusers before their arrival at the stretching extensional flow region (B). Aligned cells at equilibrium (X_{eq}) are delivered to the center of the extensional flow and deformed. (C) From high-speed videos, an automated image analysis algorithm extracts cell size and shape metrics. (D, E) Density scatter plots of size and deformability measurements, for (D) 1564 melanoma cancer cells (M395) and (E) 986 breast cancer cells (MCF7). Both cell lines have similar dimensions, but M395 are more deformable than MCF7. (F) Capture efficiency measured after processing of these cell lines through Vortex Chip reveals that less deformable MCF7 cells are more efficiently captured.

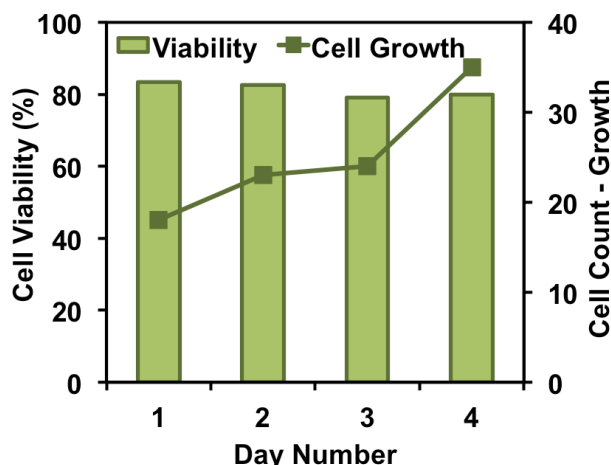


Figure SI6. Demonstration of long-term cell viability and proliferation after collection by Vortex technology. A549 lung cancer cells are captured through Vortex Chip, released, collected off-chip in a well-plate, and cultured over 3 days. Each day, cells were counted, imaged and viability assays were performed. Cell viability remains above 80% and cells successfully divide and grow over the 3-day growth period, with a doubling time of 3.1 days.

Movie 1. Particle trapping in vortices and optimal flow rate. Each movie was recorded at 6600 frames per second, with 19 μm beads injected at 1, 2.5, 4 and 6 mL/min. White arrows show interesting trajectories of individual beads. At 1 mL/min, as the vortex secondary flows are not formed in the reservoirs, the particles follow the streamwise flow, slow down in the reservoirs and return to the main channel. At 2.5 mL/min, vortices occupy a partial extent of the reservoirs. Larger particles are trapped in these vortices, where they stably recirculate. However, these vortices have a limited capacity: particle 1 (blue arrow) is pushed to an outer orbit by particle-particle interactions but comes back to its inner orbit afterwards, while particles 2 and 3 (red arrows) are pushed outside of the vortices and return to the main flow where they exit the chip. At 4 mL/min, vortices expand to occupy the entire extent of the reservoirs, providing the particles with more length and time to enter and become trapped in the vortices. As a consequence, many more particles are collected and vortices may become saturated. Particle 1 (blue arrow) illustrates this saturation of the vortices and the expulsion of a particle by particle-particle interactions. At 6 mL/min, the vortex center is shifted closer to the back of the reservoir. As shown with a red arrow, several particles may hit the back wall, enter unstable orbits and return to the main flow.

Movie 2. Vortex saturation and effect on capture stability. Both movies were recorded with high-speed microscopy, at 6600 frames per second, with 19 μm beads injected at 4 mL/min. Top: a dilute solution of beads suspended in water was injected in the device, then switched to a wash solution after

a single bead was seen trapped in the vortices. Bottom: a concentrated solution of beads was injected, then switched to wash when vortices began to saturate.

Movie 3. High-throughput and label-free collection of cancer cells from healthy human blood.

Both movies were recorded with high-speed microscopy, at 6600 frames per second, under objectives 4X (A) and 10X (B) respectively. After a preliminary PBS injection to prime the vortex flow patterns and remove air bubbles within the chip, MCF7 breast cancer cells spiked into 20X-diluted blood were injected through the Vortex Chip at 4 mL/min. Blood cells and cancer cells enter and orbit in the vortices (capture step). After sample injection, PBS is injected through the device as a washing buffer without disrupting the vortices. Blood cells are flushed away and return to the main flow while the larger cancer cells, stably trapped in the reservoirs, continue orbiting (washing step). Finally, cancer cells are released on-demand and collected into a well plate for further characterization and enumeration (release step).

References SI:

- [1] A. J. Mach, J. H. Kim, A. Arshi, S. C. Hur & D. Di Carlo. Automated cellular sample preparation using a Centrifuge-on-a-chip. *Lab Chip*, 2011, **11**, 2827-2834.
- [2] D. R. Gossett, H. T. K. Tse, S. A. Lee, Y. Ying, A. G. Lindgren, O. O. Yang, J. Rao, A. T. Clark, D. Di Carlo. Hydrodynamic stretching of single cells for large population mechanical phenotyping, *PNAS*, 2012, 109, **20**, 7630-7635.